

Can SAM Segment Polyps?

Tao Zhou, Yizhe Zhang, Yi Zhou, Ye Wu, Chen Gong

Abstract— Recently, Meta AI Research releases a general Segment Anything Model (SAM), which has demonstrated promising performance in several segmentation tasks. As we know, polyp segmentation is a fundamental task in the medical imaging field, which plays a critical role in the diagnosis and cure of colorectal cancer. In particular, applying SAM to the polyp segmentation task is interesting. In this report, we evaluate the performance of SAM in segmenting polyps, in which SAM is under unprompted settings. We hope this report will provide insights to advance this polyp segmentation field and promote more interesting works in the future. This project is publicly at <https://github.com/taozh2017/SAMPolyp>.

Index Terms—Segment anything model, colorectal cancer, polyp segmentation.



1 INTRODUCTION

LARGE Language Models (LLMs), such as ChatGPT [1] and GPT-4 [2], are pre-trained on vast amounts of text data and have demonstrated impressive performance in various natural language processing (NLP) tasks. The effectiveness of LLMs leads people to consider that how to effectively utilize these models in real-world applications. However, they are not specifically designed for image segmentation tasks [3].

Recently, Segment Anything Model (SAM) [3] is released as a general image segmentation model, which is trained on the large visual corpus (SA-1B). SAM produces high-quality object masks from input prompts (*e.g.*, points, boxes, and masks). Due to its promising performance in several segmentation tasks, SAM has attracted increasing attention to applying it to various fields. For example, Ji *et al.* [4] discussed the benefits and limitations of SAM in different computer vision and medical image segmentation tasks. Tang *et al.* [5] evaluated the performance of SAM in the field of Camouflaged Object Detection (COD). Ji *et al.* [6] evaluated SAM on three concealed scenes (*i.e.*, camouflaged animals, industrial defects, and medical lesions) under unprompted settings. Roy *et al.* [7] valuated the zero-shot capabilities of SAM on the organ segmentation task. Deng *et al.* [8] applied SAM to segment heterogeneous objects in digital pathology. The above studies show SAM can not perform well under several real-world applications. Among medical image segmentation tasks, polyp segmentation is a critical step in the diagnosis and cure of colorectal cancer. Thus, it is of great interest to investigate how well SAM can segment polyps in colonoscopy images under different challenging factors.

This report mainly evaluates the effectiveness of SAM in segmenting polyps. To achieve this, we compare SAM quantitatively and qualitatively with state-of-the-art models on the polyp segmentation task. Under the unprompted setting, it can be seen that SAM does not perform better in

the polyp segmentation task. Therefore, how to effectively apply SAM to the polyp segmentation should be further explored.

2 EXPERIMENTS AND RESULTS

2.1 Datasets

To validate the effectiveness of different polyp segmentation models, we conduct comparison experiments on five benchmark colonoscopy datasets, and the details of each dataset are introduced below. • **Kvasir** [10]: This dataset is collected by Vestre Viken Health Trust in Norway from inside the gastrointestinal tract, which consists of 1,000 polyp images. • **CVC-ClinicDB** [9]: This dataset contains 612 images collected from 29 colonoscopy video sequences with a resolution of 288×384 . • **CVC-ColonDB** [28]: This dataset consists of 380 images with a resolution of 500×570 . • **ETIS** [29]: This dataset contains 196 polyp images with a size of 966×1225 . • **CVC-300** [27]: This dataset includes 60 polyp images with a resolution of 500×574 . Following the same data split settings in [14], 900 images from Kvasir and 550 ones from CVC-ClinicDB are selected to form the training set. The remaining images from the two datasets (*i.e.*, Kvasir and CVC-ClinicDB) and the other three datasets (*i.e.*, CVC-ColonDB, ETIS, and CVC-300) are used for testing.

2.2 Experimental Settings

2.2.1 Comparison Methods

In this study, we first evaluate 14 CNN-based polyp segmentation methods, including UNet [12], UNet++ [12], SFA [13], PraNet [13], ACSNet [15], MSEG [16], DCR-Net [17], EU-Net [18], SANet [19], MSNet [20], C2FNet [21], LDNet [22], FAPNet [23], and CFA-Net [24]. Besides, we evaluate two Transformer-based segmentation models, *i.e.*, Polyp-PVT [25] and HSNet [26]. For SAM, we adopt two backbones [30] in this study, denoted as “SAM-H” and “SAM-L”, respectively.

2.2.2 Evaluation Metrics and Setting

To evaluate the effectiveness of different models, we adopt six commonly used metrics [31], [32], [33], [34], namely

• T. Zhou, Y. Zhang, Y. Wu, and C. Gong are with the School of Computer Science and Engineering, Nanjing University of Science and Technology, Nanjing, China. Y. Zhou is with the School of Computer Science and Engineering, Southeast University, Nanjing, China.

Table 1: Quantitative polyp segmentation results on the CVC-ClinicDB and Kvasir datasets. † denotes a Transformer-based model.

Methods	CVC-ClinicDB [9]						Kvasir [10]					
	mDice ↑	mIou ↑	S_α ↑	F_β^w ↑	E_ϕ^{max} ↑	\mathcal{M} ↓	mDice ↑	mIou ↑	S_α ↑	F_β^w ↑	E_ϕ^{max} ↑	\mathcal{M} ↓
UNet [11]	0.823	0.755	0.889	0.811	0.954	0.019	0.818	0.746	0.858	0.794	0.893	0.055
UNet++ [12]	0.794	0.729	0.873	0.785	0.931	0.022	0.821	0.744	0.862	0.808	0.910	0.048
SFA [13]	0.700	0.607	0.793	0.647	0.885	0.042	0.723	0.611	0.782	0.670	0.849	0.075
PraNet [14]	0.899	0.849	0.936	0.896	0.979	0.009	0.898	0.840	0.915	0.885	0.948	0.030
ACSNet [15]	0.882	0.826	0.927	0.873	0.959	0.011	0.898	0.838	0.920	0.882	0.952	0.032
MSEG [16]	0.909	0.864	0.938	0.907	0.969	0.007	0.897	0.839	0.912	0.885	0.948	0.028
DCRNet [17]	0.896	0.844	0.933	0.890	0.978	0.010	0.886	0.825	0.911	0.868	0.941	0.035
EU-Net [18]	0.902	0.846	0.936	0.891	0.965	0.011	0.908	0.854	0.917	0.893	0.954	0.028
SANet [19]	0.916	0.859	0.939	0.909	0.976	0.012	0.904	0.847	0.915	0.892	0.953	0.028
MSNet [20]	0.918	0.869	0.946	0.913	0.979	0.008	0.905	0.849	0.923	0.892	0.954	0.028
C2FNet [21]	0.919	0.872	0.941	0.906	0.976	0.009	0.886	0.831	0.905	0.870	0.935	0.036
LDNet [22]	0.881	0.825	0.924	0.879	0.965	0.012	0.887	0.821	0.905	0.869	0.945	0.031
FAPNet [23]	0.925	0.877	0.947	0.910	0.979	0.008	0.902	0.849	0.919	0.894	0.953	0.027
CFA-Net [24]	0.933	0.883	0.950	0.924	0.989	0.007	0.915	0.861	0.924	0.903	0.962	0.023
Polyp-PVT† [25]	0.948	0.905	0.953	0.951	0.993	0.006	0.917	0.864	0.925	0.911	0.962	0.023
HSNet† [26]	0.937	0.887	0.949	0.936	0.989	0.006	0.926	0.877	0.927	0.918	0.964	0.023
SAM-H [3]	0.547	0.500	0.738	0.546	0.677	0.040	0.778	0.707	0.829	0.769	0.831	0.062
SAM-L [3]	0.579	0.526	0.744	0.563	0.685	0.057	0.782	0.710	0.832	0.773	0.836	0.061

Table 2: Quantitative polyp segmentation results on the CVC-300 and ColonDB datasets. † denotes a Transformer-based model.

Methods	CVC-300 [27]						ColonDB [28]					
	mDice ↑	mIou ↑	S_α ↑	F_β^w ↑	E_ϕ^{max} ↑	\mathcal{M} ↓	mDice ↑	mIou ↑	S_α ↑	F_β^w ↑	E_ϕ^{max} ↑	\mathcal{M} ↓
UNet [11]	0.710	0.627	0.843	0.684	0.876	0.022	0.504	0.436	0.710	0.491	0.781	0.059
UNet++ [12]	0.707	0.624	0.839	0.687	0.898	0.018	0.482	0.408	0.693	0.467	0.764	0.061
SFA [13]	0.467	0.329	0.640	0.341	0.817	0.065	0.456	0.337	0.629	0.366	0.754	0.094
PraNet [14]	0.871	0.797	0.925	0.843	0.972	0.010	0.712	0.640	0.820	0.699	0.872	0.043
ACSNet [15]	0.863	0.787	0.923	0.825	0.968	0.013	0.716	0.649	0.829	0.697	0.851	0.039
MSEG [16]	0.874	0.804	0.924	0.852	0.957	0.009	0.735	0.666	0.834	0.724	0.875	0.038
DCRNet [17]	0.856	0.788	0.921	0.830	0.960	0.010	0.704	0.631	0.821	0.684	0.848	0.052
EU-Net [18]	0.837	0.765	0.904	0.805	0.933	0.015	0.756	0.681	0.831	0.730	0.872	0.045
SANet [19]	0.888	0.815	0.928	0.859	0.972	0.008	0.753	0.670	0.837	0.726	0.878	0.043
MSNet [20]	0.865	0.799	0.926	0.848	0.953	0.010	0.751	0.671	0.838	0.736	0.883	0.041
C2FNet [21]	0.874	0.801	0.927	0.844	0.968	0.009	0.724	0.650	0.826	0.705	0.868	0.044
LDNet [22]	0.869	0.793	0.923	0.841	0.965	0.009	0.740	0.652	0.830	0.717	0.884	0.036
FAPNet [23]	0.893	0.826	0.938	0.874	0.976	0.008	0.731	0.658	0.831	0.735	0.878	0.038
CFA-Net [24]	0.893	0.827	0.938	0.875	0.978	0.008	0.743	0.665	0.835	0.728	0.898	0.039
Polyp-PVT† [25]	0.900	0.833	0.935	0.884	0.981	0.007	0.808	0.727	0.865	0.795	0.919	0.031
HSNet† [26]	0.903	0.839	0.937	0.887	0.975	0.007	0.810	0.735	0.868	0.796	0.915	0.032
SAM-H [3]	0.651	0.606	0.812	0.653	0.767	0.020	0.441	0.396	0.676	0.434	0.587	0.056
SAM-L [3]	0.726	0.676	0.849	0.729	0.826	0.020	0.468	0.422	0.690	0.463	0.608	0.054

mean dice score (mDice), mean intersection over union (mIoU), S-measure (S_α) [35], F-measure [36] (F_β^w), E_ϕ^{max} [37], mean absolute error (\mathcal{M}) [38]. Due to the unprompted setting, SAM can produce multiple binary masks. Following these works [5], [6], we adopt a strategy to select the best mask based on its ground-truth map. Specifically, we have obtained N masks generated by SAM, denoted as $S_{i=1}^N$. For a given image, its ground-truth map is denoted as S . Thus, we compute S_α values for the N masks, and the mask with the highest S_α score is selected as the segmentation map.

2.3 Segmentation Results

Quantitative Comparison: Table 1, Table 2, and Table 3 show the quantitative results of different segmentation methods in the terms of six metrics on five datasets. From the results, we can observe that SAM can not effectively locate and segment polyps. On the one hand, polyp segmentation is challenging due to blurred boundaries between a polyp and its surrounding mucosa. On the other hand, SAM could be trained in a large number of natural images rather than medical images, which makes it challenging for SAM to segment polyps.

Table 3: Results on the ETIS dataset. † denotes a Transformer-based model.

	mDice \uparrow	mIou \uparrow	S_{α} \uparrow	F_{β}^w \uparrow	E_{ϕ}^{max} \uparrow	\mathcal{M} \downarrow
UNet [11]	0.398	0.335	0.684	0.366	0.740	0.036
UNet++ [12]	0.401	0.344	0.683	0.390	0.776	0.035
SFA [13]	0.297	0.217	0.557	0.231	0.633	0.109
PraNet [14]	0.628	0.567	0.794	0.600	0.841	0.031
ACSNet [15]	0.578	0.509	0.754	0.530	0.764	0.059
MSEG [16]	0.700	0.630	0.828	0.671	0.890	0.015
DCRNet [17]	0.556	0.496	0.736	0.506	0.773	0.096
EU-Net [18]	0.687	0.609	0.793	0.636	0.841	0.067
SANet [19]	0.750	0.654	0.849	0.685	0.897	0.015
MSNet [20]	0.723	0.652	0.845	0.677	0.890	0.020
C2FNet [21]	0.699	0.624	0.827	0.668	0.875	0.022
LDNet [22]	0.645	0.551	0.788	0.600	0.847	0.023
FAPNet [23]	0.717	0.643	0.841	0.657	0.884	0.019
CFA-Net [24]	0.732	0.655	0.845	0.693	0.892	0.014
Polyp-PVT† [25]	0.787	0.706	0.871	0.750	0.910	0.013
HSNet† [26]	0.808	0.734	0.882	0.777	0.909	0.021
SAM-H [3]	0.517	0.477	0.730	0.513	0.660	0.029
SAM-L [3]	0.551	0.507	0.751	0.544	0.687	0.030

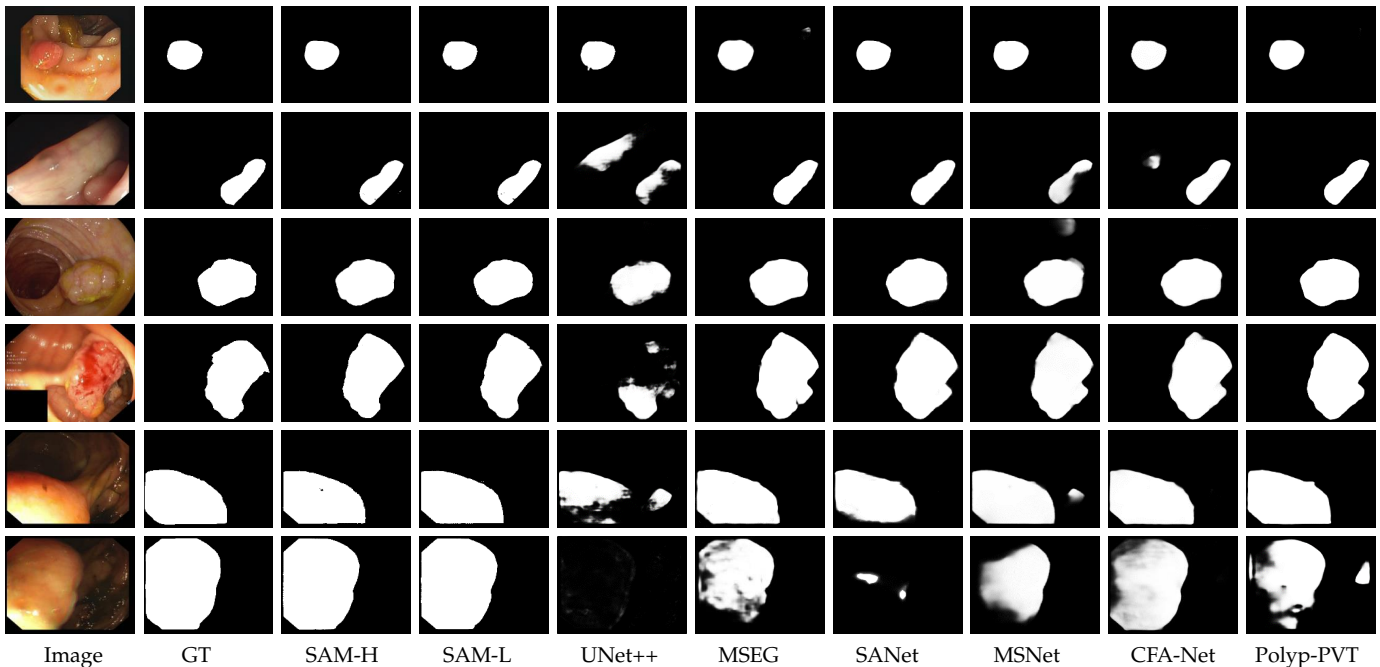


Figure 1: Some better segmentation examples of SAM.

Qualitative Comparison: We also show some better and bad segmentation examples of SAM in Fig. 1 and Fig. 2, respectively. As shown in Fig. 1, it can be seen that SAM accurately segments polyps in some scenes. However, SAM fails to segment polyps when the boundary between a polyp and its surrounding mucosa is non-sharp, as shown in the 3rd and 4th rows in Fig. 2.

3 CONCLUSION

This report provides a preliminary evaluation of SAM in segmenting polyps using colonoscopy images. We have conducted experiments on five benchmark datasets, and

the results demonstrate there is still room for improvement when applying SAM to the polyp segmentation task. It can be noted that we directly apply the trained model from SAM to infer the polyp segmentation so that it is difficult to achieve satisfactory performance for these unseen medical images. Thus, one possible solution is to fine-tune the SAM model using training datasets of the specific task. In this case, we could obtain better segmentation performance than that without a fine-tuning strategy. We hope this report will promote more interest in this field of polyp segmentation, and more research works leveraging SAM will be developed in this area. To promote future research for polyp

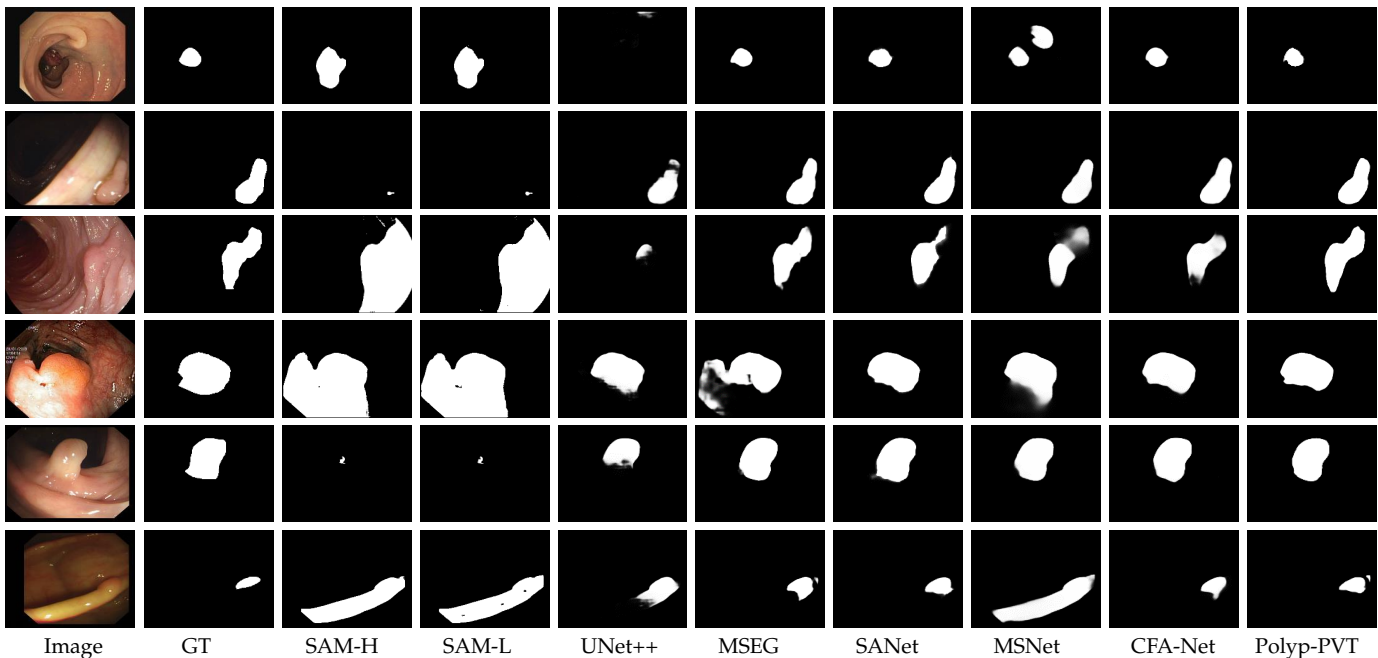


Figure 2: Some failure segmentation examples of SAM.

segmentation, we will collect awesome polyp segmentation models at: <https://github.com/taozh2017/Awesome-Polyp-Segmentation>.

REFERENCES

- [1] T. Brown, B. Mann, N. Ryder, M. Subbiah, J. D. Kaplan, P. Dhariwal, A. Neelakantan, P. Shyam, G. Sastry, A. Askell *et al.*, "Language models are few-shot learners," *Advances in neural information processing systems*, vol. 33, pp. 1877–1901, 2020.
- [2] OpenAI, "Gpt-4 technical report," 2023.
- [3] A. Kirillov, E. Mintun, N. Ravi, H. Mao, C. Rolland, L. Gustafson, T. Xiao, S. Whitehead, A. C. Berg, W.-Y. Lo *et al.*, "Segment anything," *arXiv preprint arXiv:2304.02643*, 2023.
- [4] W. Ji, J. Li, Q. Bi, W. Li, and L. Cheng, "Segment anything is not always perfect: An investigation of sam on different real-world applications," *arXiv preprint arXiv:2304.05750*, 2023.
- [5] L. Tang, H. Xiao, and B. Li, "Can sam segment anything? when sam meets camouflaged object detection," *arXiv preprint arXiv:2304.04709*, 2023.
- [6] G.-P. J. Ji, D.-P. Fan, P. Xu, M.-M. Cheng, B. Zhou, and L. Van Gool, "Sam struggles in concealed scenes-empirical study on "segment anything"," *arXiv preprint arXiv:2304.06022*, 2023.
- [7] S. Roy, T. Wald, G. Koehler, M. R. Rokuss, N. Disch, J. Holzschuh, D. Zimmerer, and K. H. Maier-Hein, "Sam. md: Zero-shot medical image segmentation capabilities of the segment anything model," *arXiv preprint arXiv:2304.05396*, 2023.
- [8] R. Deng, C. Cui, Q. Liu, T. Yao, L. W. Remedios, S. Bao, B. A. Landman, L. E. Wheless, L. A. Coburn, K. T. Wilson *et al.*, "Segment anything model (sam) for digital pathology: Assess zero-shot segmentation on whole slide imaging," *arXiv preprint arXiv:2304.04155*, 2023.
- [9] J. Bernal, F. J. Sánchez, G. Fernández-Esparrach, D. Gil, C. Rodríguez, and F. Vilariño, "WM-DOVA maps for accurate polyp highlighting in colonoscopy: Validation vs. saliency maps from physicians," *Computerized Medical Imaging and Graphics*, vol. 43, pp. 99–111, 2015.
- [10] D. Jha, P. H. Smedsrud, M. A. Riegler, P. Halvorsen, T. de Lange, D. Johansen, and H. D. Johansen, "Kvasir-seg: A segmented polyp dataset," in *Int. Conf. on Multimedia Modeling*, 2020, pp. 451–462.
- [11] O. Ronneberger, P. Fischer, and T. Brox, "U-net: Convolutional networks for biomedical image segmentation," in *Proc. Int. Conf. Med. Image Comput. Comput. Assist. Intervent.*, 2015, pp. 234–241.
- [12] Z. Zhou, M. M. R. Siddiquee, N. Tajbakhsh, and J. Liang, "Unet++: Redesigning skip connections to exploit multiscale features in image segmentation," *IEEE Trans. Med. Imaging*, vol. 39, no. 6, pp. 1856–1867, 2019.
- [13] Y. Fang, C. Chen, Y. Yuan, and K.-y. Tong, "Selective feature aggregation network with area-boundary constraints for polyp segmentation," in *Proc. Int. Conf. Med. Image Comput. Comput. Assist. Intervent.*, 2019, pp. 302–310.
- [14] D.-P. Fan, G.-P. Ji, T. Zhou, G. Chen, H. Fu, J. Shen, and L. Shao, "Pranet: Parallel reverse attention network for polyp segmentation," in *Proc. Int. Conf. Med. Image Comput. Comput. Assist. Intervent.*, 2020, pp. 263–273.
- [15] R. Zhang, G. Li, Z. Li, S. Cui, D. Qian, and Y. Yu, "Adaptive context selection for polyp segmentation," in *Proc. Int. Conf. Med. Image Comput. Comput. Assist. Intervent.* Springer, 2020, pp. 253–262.
- [16] C.-H. Huang, H.-Y. Wu, and Y.-L. Lin, "Hardnet-mseg: A simple encoder-decoder polyp segmentation neural network that achieves over 0.9 mean dice and 86 fps," *arXiv preprint arXiv:2101.07172*, 2021.
- [17] Z. Yin, K. Liang, Z. Ma, and J. Guo, "Duplex contextual relation network for polyp segmentation," in *Proc. Int. Symp. Biomed. Imaging*, 2022, pp. 1–5.
- [18] K. Patel, A. M. Bur, and G. Wang, "Enhanced u-net: A feature enhancement network for polyp segmentation," in *Proc. IEEE Int. Robots and Vision*, 2021, pp. 181–188.
- [19] J. Wei, Y. Hu, R. Zhang, Z. Li, S. K. Zhou, and S. Cui, "Shallow attention network for polyp segmentation," in *Proc. Int. Conf. Med. Image Comput. Comput. Assist. Intervent.* Springer, 2021, pp. 699–708.
- [20] X. Zhao, L. Zhang, and H. Lu, "Automatic polyp segmentation via multi-scale subtraction network," in *Proc. Int. Conf. Med. Image Comput. Comput. Assist. Intervent.*, 2021, pp. 120–130.
- [21] Y. Sun, G. Chen, T. Zhou, Y. Zhang, and N. Liu, "Context-aware cross-level fusion network for camouflaged object detection," in *Proceedings of the Proc. Int. Jt. Conf. Artif. Intell.*, 2020, pp. 1025–1031.
- [22] R. Zhang, P. Lai, X. Wan, D.-J. Fan, F. Gao, X.-J. Wu, and G. Li, "Lesion-aware dynamic kernel for polyp segmentation," in *Proc. Int. Conf. Med. Image Comput. Comput. Assist. Intervent.* Springer, 2022, pp. 99–109.
- [23] T. Zhou, Y. Zhou, C. Gong, J. Yang, and Y. Zhang, "Feature aggregation and propagation network for camouflaged object detection," *IEEE Trans. Image Process.*, vol. 31, pp. 7036–7047, 2022.
- [24] T. Zhou, Y. Zhou, K. He, C. Gong, J. Yang, H. Fu, and D. Shen, "Cross-level feature aggregation network for polyp segmentation," *Pattern Recognition*, p. 109555, 2023.

- [25] B. Dong, W. Wang, D.-P. Fan, J. Li, H. Fu, and L. Shao, "Polyp-pvt: Polyp segmentation with pyramid vision transformers," *arXiv preprint arXiv:2108.06932*, 2021.
- [26] W. Zhang, C. Fu, Y. Zheng, F. Zhang, Y. Zhao, and C.-W. Sham, "Hsnet: A hybrid semantic network for polyp segmentation," *Computers in Biology and Medicine*, vol. 150, p. 106173, 2022.
- [27] D. Vázquez, J. Bernal, F. J. Sánchez, G. Fernández-Esparrach, A. M. López, A. Romero, M. Drozdal, and A. Courville, "A benchmark for endoluminal scene segmentation of colonoscopy images," *Journal of Healthcare Engineering*, pp. 1–9, 2017.
- [28] N. Tajbakhsh, S. R. Gurudu, and J. Liang, "Automated polyp detection in colonoscopy videos using shape and context information," *IEEE Trans. Med. Imaging*, vol. 35, no. 2, pp. 630–644, 2015.
- [29] J. Silva, A. Histace, O. Romain, X. Dray, and B. Granado, "Toward embedded detection of polyps in wce images for early diagnosis of colorectal cancer," *Int. J. of Computer Assist. Radiology and Surgery*, vol. 9, no. 2, pp. 283–293, 2014.
- [30] A. Dosovitskiy, L. Beyer, A. Kolesnikov, D. Weissenborn, X. Zhai, T. Unterthiner, M. Dehghani, M. Minderer, G. Heigold, S. Gelly *et al.*, "An image is worth 16x16 words: Transformers for image recognition at scale," *arXiv preprint arXiv:2010.11929*, 2020.
- [31] C. Yang, X. Guo, M. Zhu, B. Ibragimov, and Y. Yuan, "Mutual-prototype adaptation for cross-domain polyp segmentation," *IEEE J. Biomed. Health Informat.*, vol. 25, no. 10, pp. 3886–3897, 2021.
- [32] T. Zhou, D.-P. Fan, M.-M. Cheng, J. Shen, and L. Shao, "RGB-D salient object detection: A survey," *Computational Visual Media*, vol. 7, no. 1, pp. 37–69, 2021.
- [33] T. Zhou, H. Fu, G. Chen, Y. Zhou, D.-P. Fan, and L. Shao, "Specificity-preserving rgb-d saliency detection," in *Proc. IEEE Int. Conf. Comput. Vis.*, 2021, pp. 4681–4691.
- [34] D.-P. Fan, G.-P. Ji, G. Sun, M.-M. Cheng, J. Shen, and L. Shao, "Camouflaged object detection," in *Proc. IEEE Conf. Comput. Vis. Pattern Recognit.*, 2020, pp. 2777–2787.
- [35] M.-M. Chen and D.-P. Fan, "Structure-measure: A new way to evaluate foreground maps," *Int. J. Comput. Vis.*, vol. 129, pp. 2622–2638, 2021.
- [36] R. Achanta, S. Hemami, F. Estrada, and S. Susstrunk, "Frequency-tuned salient region detection," in *Proc. IEEE Conf. Comput. Vis. Pattern Recognit.*, 2009, pp. 1597–1604.
- [37] D.-P. Fan, C. Gong, Y. Cao, B. Ren, M.-M. Cheng, and A. Borji, "Enhanced-alignment measure for binary foreground map evaluation," in *Proc. Int. Jt. Conf. Artif. Intell.*, 2018, pp. 698–704.
- [38] F. Perazzi, P. Krähenbühl, Y. Pritch, and A. Hornung, "Saliency filters: Contrast based filtering for salient region detection," in *Proc. IEEE Conf. Comput. Vis. Pattern Recognit.*, 2012, pp. 733–740.